



HAL
open science

Multiscale simulation and experimental analysis of damping in CFRP structures containing rubber

Y El Archi, N Lahellec, Stéphane Lejeunes, A Jouan, B Tranquart

► To cite this version:

Y El Archi, N Lahellec, Stéphane Lejeunes, A Jouan, B Tranquart. Multiscale simulation and experimental analysis of damping in CFRP structures containing rubber. *Composite Structures*, 2022, 289, pp.115456. 10.1016/j.compstruct.2022.115456 . hal-04163486

HAL Id: hal-04163486

<https://hal.science/hal-04163486>

Submitted on 17 Jul 2023

HAL is a multi-disciplinary open access archive for the deposit and dissemination of scientific research documents, whether they are published or not. The documents may come from teaching and research institutions in France or abroad, or from public or private research centers.

L'archive ouverte pluridisciplinaire **HAL**, est destinée au dépôt et à la diffusion de documents scientifiques de niveau recherche, publiés ou non, émanant des établissements d'enseignement et de recherche français ou étrangers, des laboratoires publics ou privés.

Multiscale simulation and experimental analysis of damping in CFRP structures containing rubber

Y. El Archi^{a,b,*}, N. Lahellec^a, S. Lejeunes^a, A. Jouan^b, B. Tranquart^b

^a*LMA, UMR 7031, Aix-Marseille Univ, CNRS, Centrale Marseille, Marseille, France*

^b*Safran composites, Itteville, France*

Abstract

This paper gives an intuitive numerical multi-scale method to estimate damping in anisotropic viscoelastic hybrid composite structures using finite element analysis. Different CFRP-R (CFRP with Rubber) architectures, both microstructural and macrostructural, are studied and compared in order to maximize damping but also to minimize rigidity loss. Homogenization by virtual DMA in frequency domain is performed on representative volume elements (RVE) to obtain the effective viscoelastic behaviour of every hybrid microstructure. The effective behaviours are used to define mechanical behaviour of laminates on which vibratory simulations are performed. Interesting and advanced simulations are discussed regarding materials parameters and geometrical aspects and are compared to experimental results.

Key words: viscoelasticity, homogenization, dynamical mechanical analysis, CFRP damping

1. Introduction

In aeronautics, the latest generations of turbojets have inlet fan blades made of 3D-woven carbon fibre composite. Damping of rotating structures, such as blades, is of major industrial concern for controlling vibratory instabilities, like in-flight flutter for example, which can lead to the degradation of these blades (see Marshall and Imregun [32] for a review on the aeroelastic effects on turbomachine blades or more recently Vahdati et al. [47] which shows that flutter is still of major concern for modern aircraft engines). These kind of instabilities occur at relatively low frequencies, i.e. around the first, second and third (maximum) eigenmodes of blades. In order to overcome this difficulty, it seems necessary to implement innovative solutions to improve the damping of such a structure. Different ways of improving damping exist, this study focuses on the addition of a dissipative elastomer material in the structure. Hence, this study is devoted to the estimation of damping properties of hybrid composite laminates made with epoxy resin, elastomer and carbon fibres.

In this study, three ways to introduce the elastomer within the structure, leading to three different technologies, are studied : The first technology consists in the bonding of an elastomeric layer at the scale of the laminate structure which is also known as the viscoelastic **patch** (see Jones [23] or Martinez-Agirre et al. [33]). Here the solution studied is a particular case for which the elastomer layer lies within the laminate which is called as the constrained layer damping. This passive damping technology is commonly used in the automotive or aeronautical industries and has been widely studied and applied on CFRP laminates (Yim and Gillespie Jr [50], Kishi et al. [26], Kulhavy et al. [28], Zheng et al. [51]) The second technology, named **co-fabric** in the following, consists in the introduction of some elastomeric fibres in the carbon fabric at the microscale. This kind of fibre-hybrid composite is used for its capability of adding the properties of different types of fibre (see Swolfs et al. [44] for a review). However, few works deal with the mixing of carbon

*Corresponding author

Email addresses: elarchi@lma.cnrs-mrs.fr, tel: +33484525597 (S. Lejeunes)

with elastomer fibres in order to optimize the damping properties. Martone et al. [34] studied hybrid UD composites made with polyurethane (PU) and carbon fibres at 2.5% and 5% volume fraction of PU fibres. The damping properties of the hybrid composites are measured by using 3 points bending DMA tests. Evolutions of the complex moduli along the longitudinal and transverse directions of the UD are compared for the ply with different PU content and a reference UD without PU fibres. A significant enhancement of the damping properties is pointed out on both principal directions for the highest PU content but it also goes along with a surprisingly high loss of modulus along fibres direction. In the last technology, still at the microscale, all the carbon fibres are **coated** with a thin layer of elastomer. Hwang and Gibson [22] or Kern et al. [25] studied the influence of the interface between carbon continuous fibres and the epoxy matrix in unidirectional composites using finite elements simulations on representative volume elements. Given the mechanical properties considered, the authors enlighten the impact of such an interface material on damping properties. Finegan and Gibson [15] were, to the authors' knowledge, the first to consider highly dissipative coating for damping estimation. As was done by Hwang and Gibson [22], they compute the loss factor of the composite material defined by a given representative volume element and by using a finite element method. From an experimental point of view, Gao et al. [17] made some dynamic testing on 3D braided composite, with carbon fibres coated by nitrile rubber, and they noticed the influence of the coating on the material's damping response.

Assuming the infinitesimal strain theory, the dissipative behaviour of the epoxy resin and the rubber material used in this study, is modelled in the framework of linear viscoelasticity (Gurtin and Sternberg [18], Roylance [42], Knauss et al. [27], Diani and Gilormini [11]). Such behaviour is characterized by a high dependency of the mechanical properties on the loading frequency and temperature which can be related by the time and temperature superposition principle (Ferry [14]). DMA (Dynamic Mechanical Analysis) tests (Bert [2], Lakes [29]) can be used to characterize the damping properties through the steady state response of the material to harmonic loading which can be modelled in the frequency domain by a set of complex elastic moduli. Very rich literature is available on the topic of DMA testing, for example Dealy and Plazek (Dealy and Plazek [10]) successfully use this measurement method and the time-temperature superposition principle (Williams et al. [49]) to build the master curve of the complex shear modulus μ^* over a wide range of frequencies for a blend of two linear polybutadienes. One of the challenging points in DMA testing today is to measure simultaneously two independent complex moduli to get the full response of isotropic material and to have indirectly access to the complex Poisson's ratio (Tschoegl et al. [46], Pritz [40]). When only one test is available, it is often assumed that the Poisson's ratio remains constant according to frequency (see for example O'Brien et al. [38], El Mourid et al. [13] or Courtois et al. [9]).

Knowing the local constituents (carbon fibres, epoxy resin and rubber) behaviours and the microstructure (arrangement of the different constituents with respect to each other), the plies behaviour can be estimated by using an homogenization method. In the framework of linear viscoelasticity, the easiest way is to use the Laplace-Carson transform and the so-called correspondence principle (Schapery [43]). The local material behaviours are defined by their complex elastic moduli and the macroscopic response can be obtained by well known linear homogenization methods in the frequency domain. The mean field methods give access to the macroscopic response in closed form (Hashin [20], Rougier et al. [41] and Schapery [43]) but they are limited to idealized microstructures not necessarily representative of the industrial composites that we are interested in. On the other hand, the full field methods can be used to solve numerically the homogenization equations on a representative volume element characterizing the composite microstructure (see El Hachemi et al. [12] and Liebig et al. [31] which used finite elements method and Noûs et al. [37] which applied a numerical method based on Fast Fourier Transforms).

The plies behaviour being known, by using a homogenization method or experimental measurements, two main techniques based on the Finite Element Method can be used to estimate the damping of composite structures: In the first one, named strain energy approach, for a given frequency, the damping of the structure is related to the ratio between the dissipated energy over one cycle and the strain energy (see Berthelot et al. [3], Yim and Gillespie Jr [50] or Pereira et al. [39] for some applications to laminated composites structures). In the second one, using the correspondence principle, linear FEM calculations are done in the frequency domain and the modal damping can be estimated by the complex eigenfrequencies of the system, see Kern et al. [25] or He et al. [21], or by the bandwidth around each eigenfrequency of the frequency spectrum, as

can be done experimentally.

In the present work, the damping of CFRP structures is estimated by two-scales simulations: At the microscopic scale, full field simulations (using a FEM code) give the linear visco-elastic response, in the frequency domain, of the different studied plies (standard, co-fabric and coated). At the macroscopic scale, FEM simulations, still performed in the frequency domain, are used to evaluate the modal damping of structures made of different stacking of these plies.

The paper is organized as follows. Section 2 concerns the local constituents behaviour. The carbon fibres are assumed to be linear elastic and the epoxy resin and the rubber are assumed to follow linear viscoelastic laws identified by DMA test results. Section 3 concerns the homogenization procedure used to estimate the plies behaviour. A preliminary step of representative volume element (RVE) definition for each technology is cautiously realized and analysed according to the expected transversely isotropic behaviour at the ply scale. This homogenization step is achieved numerically by simulating virtual DMA tests on RVEs with the finite elements commercial code Abaqus using the "Steady-State Dynamics - Direct" procedure (El Hachemi et al. [12] and Liebig et al. [31]). With this same procedure, but at the laminate scale, the damping properties of the different structures are estimated by simulating cantilever beam vibration tests (Nashif et al. [36]) in section 4. This testing method is commonly used and gives access to the structural damping ratio ξ (Kishi et al. [26], Kulhavy et al. [28]).

2. Individual constituents local mechanical behaviour

2.1. Microstructure description

Two different technologies containing elastomer at the microscale are studied. In both microstructures the contents of fillers (volume fractions) are the same and are given in Table 1.

material	volume fraction f (%)	density (g/cm^3)
Epoxy	45	1.2
Carbon	50	1.78
Rubber	5	1.5

Table 1: Volume fractions and densities of every RVE constituent

Three microstructures are studied, for which cross-sections along the transverse plane are shown in Figure 1: (a) concerns the UD ply without any rubber, (b) microstructure including co-fabric rubber fibres and (c) microstructure for which the carbon fibres are coated with rubber.

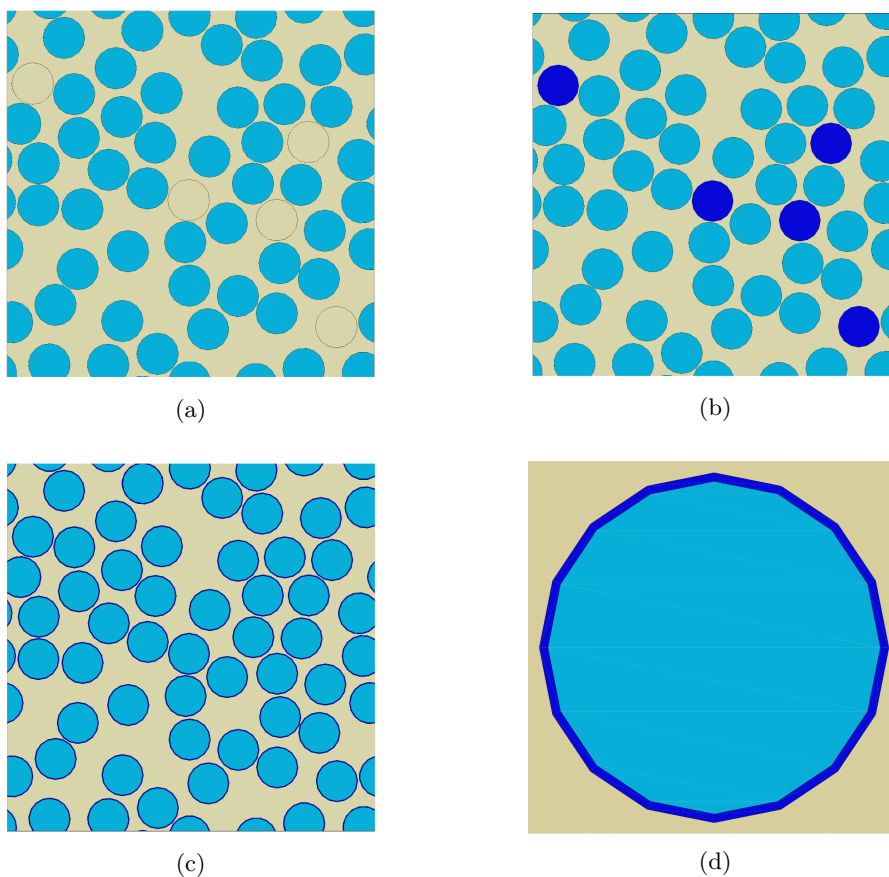


Figure 1: RVEs: (a) "Reference" microstructure: Contains only resin and carbon fibres. (b) "Co-fabric" microstructure: Elastomer fibres are introduced in the same direction as the carbon fibres and also possess the same geometric properties. (c) "Coated" microstructure: Every carbon fibre is coated with a thin layer of viscoelastic rubber (zoom on figure (d)).

2.2. Carbon fibres behaviour

The Carbon fibres are considered purely elastic with transversely isotropic symmetry. Their elastic properties are given in Table 2 with subscripts L and T referring respectively to the longitudinal and

transverse directions (see Courtois [8]) .

E_T	10300 MPa
E_L	310000 MPa
ν_{TT}	0.3
ν_{TL}	0.01
G_{TL}	27900 MPa

Table 2: Carbon fibres elastic properties

2.3. Epoxy resin and rubber behaviour

The local response $\boldsymbol{\sigma}(t)$ of a non ageing linear viscoelastic material to a loading strain history $\boldsymbol{\varepsilon}(u)$ ($u \in [0, t]$) (not containing any jump) can be formulated with the Stieltjes convolution products as:

$$\boldsymbol{\sigma}(t) = (\mathbf{L} * \boldsymbol{\varepsilon})(t) = \int_0^t \mathbf{L}(t-u) : \dot{\boldsymbol{\varepsilon}}(u) du, \quad (1)$$

with $\mathbf{L}(t)$ the fourth-order tensor of relaxation functions. Using the correspondence principle and the Laplace-Carson transform, see Gurtin and Sternberg [18] or Schapery [43], the constitutive law given in the time domain by (1) is transformed in a linear elastic kind relation in the Laplace domain as:

$$\hat{\boldsymbol{\sigma}}(p) = \hat{\mathbf{L}}(p) : \hat{\boldsymbol{\varepsilon}}(p), \quad (2)$$

in which $\hat{h}(p)$ denotes the Laplace-Carson transform of the function $h(t)$. In the particular case of harmonic loading (with frequency f), which is of interest in this study, the steady state response of the material can be given by (2) taking the special value $p = i\omega = i2\pi f$ with i the imaginary unit ($i^2 = -1$), see Burgarella et al. [6] or Gallican and Brenner [16] among others. This gives the constitutive law in the spectral domain:

$$\boldsymbol{\sigma}^*(f) = \mathbf{L}^*(f) : \boldsymbol{\varepsilon}^*(f), \quad (3)$$

with $h^*(f)$ the complex amplitude of the harmonic function $h(t)$ defined by $h^*(f) = \hat{h}(i2\pi f)$. $\mathbf{L}^*(f)$, usually called the tensor of complex moduli, can be identified with DMA tests, see Burgarella et al. [6]. In case of isotropic material, which is the case of the epoxy resin and the rubber studied here, it can be defined with two scalars μ^* and k^* , respectively the complex shear and bulk moduli.

Torsional DMA tests were performed according to the standard **ISO6721-7** and with the ARES G2 (TA Instruments) electromagnetic test machine to characterize the epoxy resin and the rubber complex shear modulus μ^* defined by :

$$\mu^* = \mu' + i\mu'', \quad \mu' = C \frac{T_0}{\alpha_0} \cos(\phi) \quad \text{and} \quad \mu'' = C \frac{T_0}{\alpha_0} \sin(\phi), \quad (4)$$

with, μ' and μ'' , the storage and loss shear moduli, α_0 , T_0 respectively the amplitudes of the angle of twist applied to the sample and of the torque measured, ϕ the phase lag between the angle twist and the torque signals and C a scalar characterising the sample geometry. The dimensions of the samples are 45mm length (i.e. distance between the grips) and a $3 \times 5mm^2$ rectangular cross-sectional area.

Master curves were obtained by applying the time-temperature superposition principle for the horizontal shift factors according to the test temperature (Williams et al. [49]) which give access to evolutions on a very large frequency range. The shift factors are given on figure 2 for the epoxy resin and the rubber. The reference temperature, i.e. the temperature for which the shift factor is equal to 1, is 20° C for both the resin and the rubber.

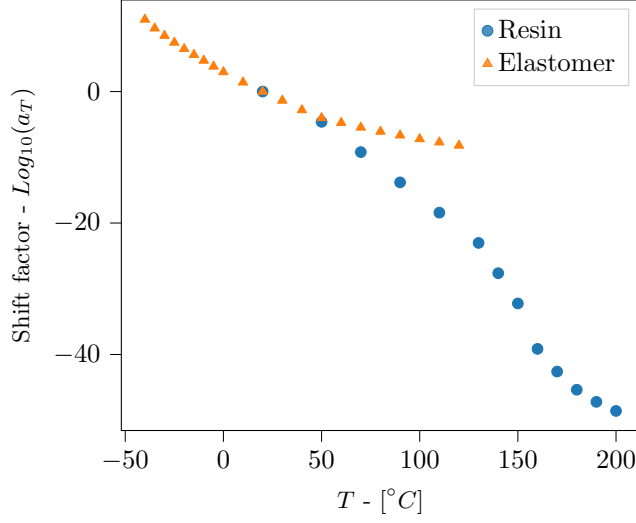


Figure 2: Shift factors used to build DMA master curves of resin and elastomer.

The master curves of the epoxy resin and the elastomer are given figure 3(a) and 3(b). Due to the WLF shifting procedure, the shear modulus is available on a very large frequency spectrum, which is called reduced frequency: $f_{red} = a_T f$.

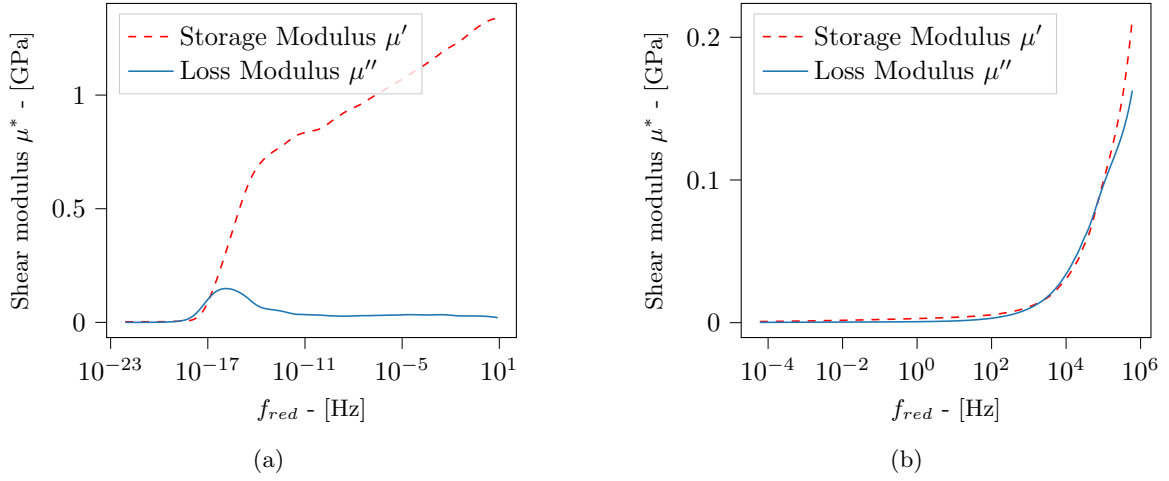


Figure 3: Master curves obtained from torsion DMA testing of resin (a) and elastomer (b)

Because of the lack of experimental data for the bulk modulus, it was estimated by assuming a real and constant Poisson's ratio with respect to the frequency as :

$$k^* = \frac{2\mu^*(1 + \nu)}{3(1 - 2\nu)} \quad (5)$$

with the values of ν given in the Table 3. Although this assumption may seem rough, it has already been widely used in the literature (see for example O'Brien et al. [38], El Mourid et al. [13] or Courtois et al. [9]).

material	Poisson's ratio
Epoxy	0.398
Rubber	0.4998

Table 3: Poisson's ratio for epoxy and rubber

3. Plies linear viscoelastic behaviour

3.1. Homogenization methodology

The plies are compound with epoxy resin reinforced with continuous carbon fibres whose diameter is very small (about $5\mu\text{m}$) with respect to the plies dimensions ($150\mu\text{m}$ thick). It is therefore impossible to implement the whole microstructure description in the FEA simulations regarding computational/numerical costs. Since the scale of the heterogeneities (carbon fibres) is very small compared to that of the plies (thickness), the principle of scale separation can be assumed and the different plies can be seen at the structure scale as some homogeneous materials, the behaviour of whom are obtain by using an homogenization method.

The damping properties of the different studied structures will be estimated with dynamical simulations. When the wavelengths associated with the displacement field are much larger than the heterogeneities' size, the homogenization can be done in the quasistatic limit, see Milton [35], this hypothesis is verified in the present study where only the first and second vibration modes are investigated. Which means that the mechanical effective properties of the plies can be obtained with static computations done at the microscale and the results will be used in the dynamical computations at the macroscale (scale of the structure), the plies density being the volume average¹ of the local constituents densities as :

$$\tilde{\rho} = \langle \rho(\mathbf{x}) \rangle = \sum_{r=1}^N c^{(r)} \rho^{(r)}, \quad (6)$$

with N the number of constituents (phases) in the ply (2 for the case without rubber and 3 for the case with rubber), $c^{(r)}$ and $\rho^{(r)}$ respectively the volume fraction and the density of constituent r .

The steady state effective response of the plies, to an applied macroscopic harmonic strain ² defined by a frequency f and a complex amplitude $\bar{\boldsymbol{\varepsilon}}^*$, is defined by the effective tensor of complex moduli $\tilde{\mathbf{L}}^*$, through the relation:

$$\bar{\boldsymbol{\sigma}}^* = \tilde{\mathbf{L}}^* : \bar{\boldsymbol{\varepsilon}}^*, \quad (7)$$

with $\bar{\boldsymbol{\sigma}}^* = \langle \boldsymbol{\sigma}^*(\mathbf{x}, f) \rangle$ and $\boldsymbol{\sigma}^*(\mathbf{x}, f)$ solution of the homogenization problem in the spectral domain, see for example Gallican and Brenner [16] :

$$\begin{cases} \text{div}(\boldsymbol{\sigma}^*(\mathbf{x}, f)) = 0 & \forall \mathbf{x} \in V, \\ \boldsymbol{\sigma}^*(\mathbf{x}, f) = \mathbf{L}^*(\mathbf{x}, f) : \boldsymbol{\varepsilon}^*(\mathbf{x}, f) & \forall \mathbf{x} \in V, \\ \langle \boldsymbol{\varepsilon}^* \rangle = \bar{\boldsymbol{\varepsilon}}^* & + \text{periodic boundaries conditions.} \end{cases} \quad (8)$$

In equation (8), V is a representative volume element (denoted RVE in the following) which definition process is detailed in paragraph 3.2. It must be representative of the studied microstructures, see figure 4 for an example of such a UD ply. $\tilde{\mathbf{L}}^*$ is identified by solving the equations system (8) by applying 6 elementary loads. Since the distribution of fibres is statistically isotropic in the transverse plane, the plies are assumed to be transversely isotropic. Then, $\tilde{\mathbf{L}}^*$ can be defined in the Walpole basis with 5 independent moduli (Bornert et al. [4], Burgarella et al. [6]) as written in equation 3.1. It is a projection on a basis of symmetrical and orthogonal 4th order tensors except for \mathbb{F} which is not symmetrical and does not verify

¹ $\langle f(\mathbf{x}) \rangle$ denotes the volume average of field f in the representative volume element V : $\langle f(\mathbf{x}) \rangle = \frac{1}{|V|} \int_V f(\mathbf{x}) \, \text{d}\mathbf{x}$.

²This procedure can also be used with an applied macroscopic $\bar{\boldsymbol{\sigma}}^*$ or a combination of $\bar{\boldsymbol{\varepsilon}}^*$ and $\bar{\boldsymbol{\sigma}}^*$

the property of projectors ($\mathbf{P} : \mathbf{P} = \mathbf{P}$). The tensor \mathbf{F} allows to describe the Poisson effect, i.e. the coupling between an elongation along the symmetry axis and a contraction in the transverse plane.

$$\tilde{\mathbf{L}}^* = \tilde{\alpha}^* \mathbf{E}_L + \tilde{\beta}^* \mathbf{J}_T + \tilde{\gamma}^* (\mathbf{F} + \mathbf{F}^T) + \tilde{\delta}_T^* \mathbf{K}_T + \tilde{\delta}_L^* \mathbf{K}_L. \quad (9)$$

The set of moduli ($\tilde{\alpha}^*, \tilde{\beta}^*, \tilde{\gamma}^*, \tilde{\delta}_T^*, \tilde{\delta}_L^*$) is convenient because it directly gives access to the tensor coefficients but it can also be used to express the engineering constants (Young modulus, Poisson coefficient and shear modulus according to longitudinal and transverse directions):

$$\tilde{E}_T^* = \frac{2\tilde{\alpha}^* \tilde{\beta}^* \tilde{\delta}_T^* - (\tilde{\gamma}^*)^2 \tilde{\delta}_T^*}{\tilde{\alpha}^* (\tilde{\beta}^* + \tilde{\delta}_T^*) - (\tilde{\gamma}^*)^2}, \quad \tilde{E}_L^* = \tilde{\alpha}^* - \frac{(\tilde{\gamma}^*)^2}{\tilde{\beta}^*}, \quad \tilde{\nu}_{TT}^* = \frac{\tilde{\alpha}^* \tilde{\beta}^* - (\tilde{\gamma}^*)^2 - \tilde{\alpha}^* \tilde{\delta}_T^*}{\tilde{\alpha}^* \tilde{\beta}^* - (\tilde{\gamma}^*)^2 + \tilde{\alpha}^* \tilde{\delta}_T^*}, \quad \tilde{\nu}_{TL}^* = \frac{\tilde{\gamma}^*}{\sqrt{2} \tilde{\beta}^*}, \quad \tilde{\mu}_{TL}^* = \frac{\tilde{\delta}_L^*}{2} \quad (10)$$

In practice, the FEA software Abaqus can be used to solve this problem in an analogous way as an elastic problem with "Direct-solution steady-state dynamic analysis" solver. The elastic properties of table 2 were used to define the carbon fibre behaviour, the real and imaginary part of the complex shear and bulk moduli μ^* and k^* respectively given by the DMA test results plotted in Figure 3 and formulae (5) were used as direct input data for the epoxy resin and the rubber behaviour with a UMAT subroutine. The periodic boundary conditions (PBC) were imposed using Homtools (see Lejeunes and Bourgeois [30]) which allows to straightforwardly impose and compute the (real or complex) macroscopic strain or stress.

3.2. Definition of a RVE

In real cross section microstructure of UD composites, fibres are not perfectly equidistantly distributed due to curing procedures for example. Which is why a proper study on the convergence of the mechanical properties according to the size of the RVE is needed. Figure 4 extracted from Alberola and Benzarti [1] shows an example of distribution of fibres in a unidirectional composite.

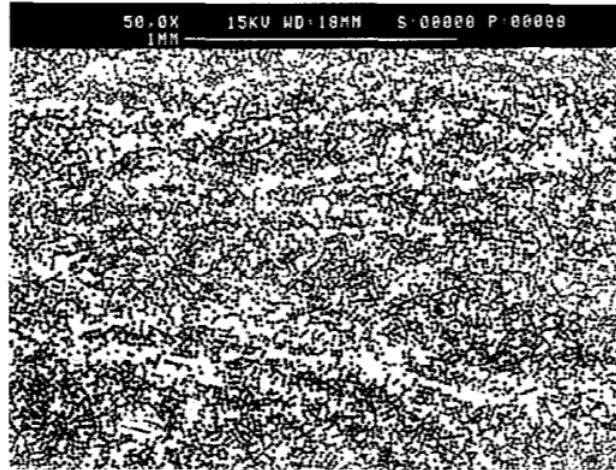


Figure 4: Scanning electron microscope observation of glass fibres distribution in a unidirectional composite made with 48% glass fibres and 52% epoxy resin given by (Alberola and Benzarti [1]).

Two convergence studies are carried out to firstly determine a mesh element size and secondly a RVE size large enough to be representative of the composite behaviour, as done in Gusev [19] for example.

These studies are carried out in the particular case where the viscoelastic tensor \mathbf{L}^* of every constituent is purely real, which, equivalently, means that only elasticity parts of their behaviour are considered. The algorithm used to generate the microstructures is of RSA type (Random Sequential Addition) which randomly

and sequentially places the spherical objects avoiding inter-penetrability in the defined volume (Torquato and Haslach [45]).

Both convergence studies were performed on two-phase material made with carbon and epoxy resin. Elastic properties used for carbon are defined on table 2 and for the epoxy resin the following elastic properties are considered.

$$\begin{cases} E^M = 7.5 \text{ MPa} \\ \nu^M = 0.398 \end{cases} \quad (11)$$

The Young modulus E^M considered for the resin is calculated using the value of shear modulus at very low frequencies (cf. figure 3a) so that the highest contrast exists between the resin and the carbon properties. Many authors have shown that the lowest convergence rates happen for the highest (stiffness) contrasts (Kanit et al. [24], Bornert et al. [5]). It is assumed that the convergence results obtained with this set of parameters will therefore be valid for any smaller contrast.

3.2.1. Determination of the Mesh density

A macroscopic stress is applied on the RVE shown in figure (1a). As outputs, we extract the macroscopic strains along the loading directions. A generalized plane strain element type was used for the simulations, therefore, even if the model is bi-dimensional, 4 different loading cases were studied: $\bar{\sigma}_{11}$, $\bar{\sigma}_{22}$, $\bar{\sigma}_{33}$ and $\bar{\sigma}_{12}$. An error estimation is introduced to compare the results to a reference mesh that is considered fine enough to obtain results close to the real behaviour.

$$E_k = \frac{|\bar{\varepsilon}_{ij,N} - \bar{\varepsilon}_{ij,k}|}{\bar{\varepsilon}_{ij,N}} \quad (12)$$

Where $\bar{\varepsilon}_{ij,N}$ stands for macroscopic strain value of the finest mesh that is close enough to the exact solution, and $ij \in \{11, 22, 33, 12\}$. $\bar{\varepsilon}_{ij,k}$ corresponds to the macroscopic strain for the mesh k whose mesh size is bigger than the mesh of index N . The graphs on figure 5 represent the strain along the same direction as the applied load according to the different meshes (denoted from 1 to $N = 6$, mesh 6 is the reference which explains the 0 error for this mesh).

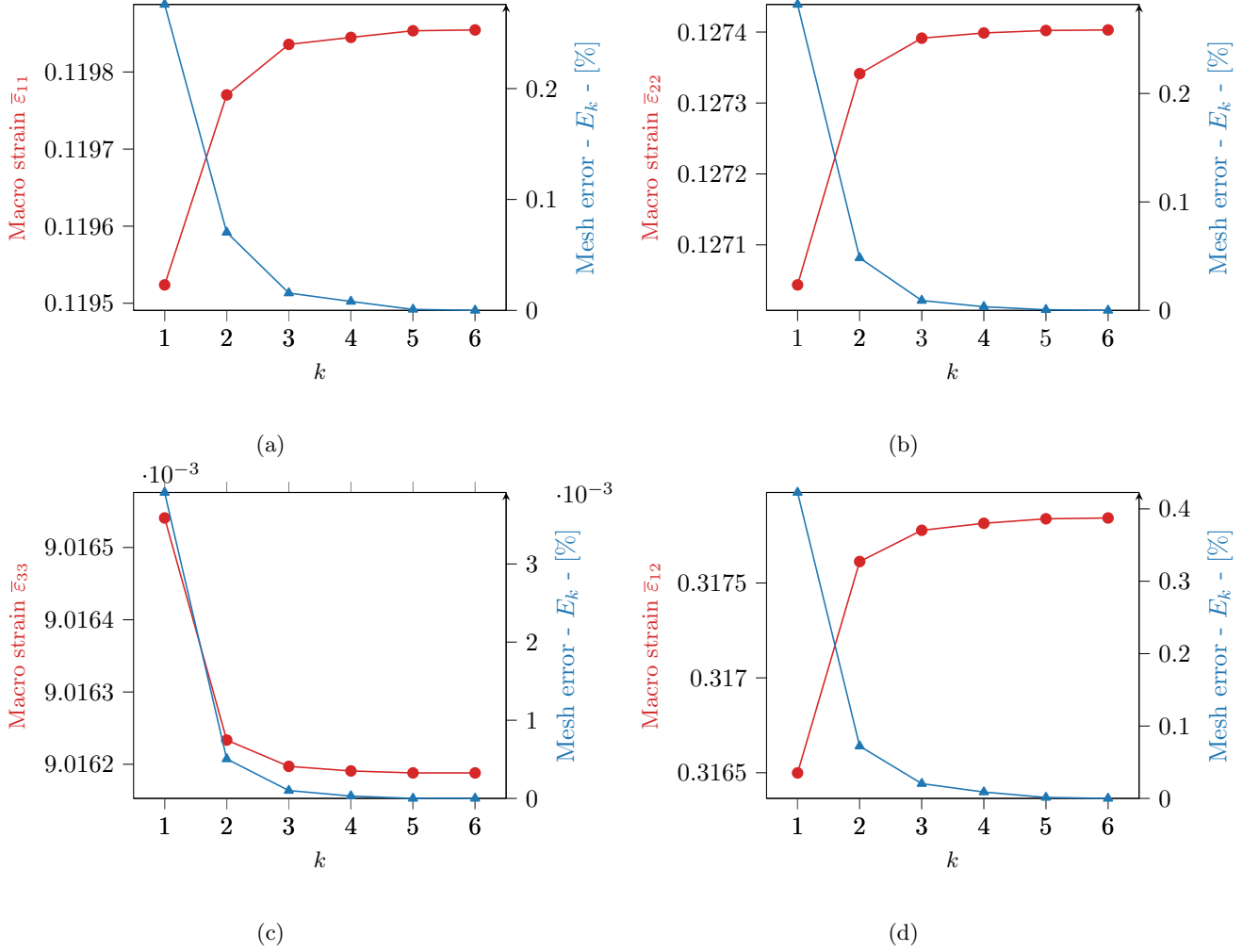


Figure 5: Macroscopic strain value and its associated error in different loading cases: tension stress $\bar{\sigma}_{11}$ (a), tension stress $\bar{\sigma}_{22}$ (b), tension stress $\bar{\sigma}_{33}$ (c) and shear stress $\bar{\sigma}_{12}$ (d). The abscissa, noted k , corresponds to a mesh size that decreases as k increases.

These results show that mesh convergence for the macroscopic quantities can be assured for every draw of microstructure tested. The element size corresponding to mesh $k = 4$ was selected to continue the simulations because it respects the criterion $E_4 < 0.01\% \quad \forall \bar{\sigma}_{ij}$.

3.2.2. RVE size determination

A statistical study was carried out to determine the optimum RVE size according to the following procedure. A large number of RVEs populations with more and more fibres but the same volume fraction was built. Every population contains ten draws of RVEs. On each RVE, 4 elementary loading cases, similar to the ones explained in paragraph 3.2.1, were applied. The homogenized 2D elasticity tensor $\tilde{\mathbf{L}}$ and its orthogonal projection $\tilde{\mathbf{L}}^p$ was then computed numerically using 13.

$$\tilde{\mathbf{L}}^p = (\mathbf{E}_L :: \tilde{\mathbf{L}})\mathbf{E}_L + (\mathbf{J}_T :: \tilde{\mathbf{L}})\mathbf{J}_T + (\mathbf{F}^T :: \tilde{\mathbf{L}})(\mathbf{F} + \mathbf{F}^T) + \frac{1}{2}(\mathbf{K}_T :: \tilde{\mathbf{L}})\mathbf{K}_T. \quad (13)$$

Where $\mathbf{A} :: \mathbf{B} = A_{ijkl}B_{lkji}$ in Einstein notation. The evolution of the error to perfectly transversely isotropic tensor according to the number of fibres contained in the RVE is presented on figure 6. For each number of fibres, 10 draws of RVEs were generated in order to obtain statistically representative results. This graph

shows that the error is globally small regardless of the number of fibres. However, in the continuation of the study, it was chosen to work on RVEs containing 55 fibres.

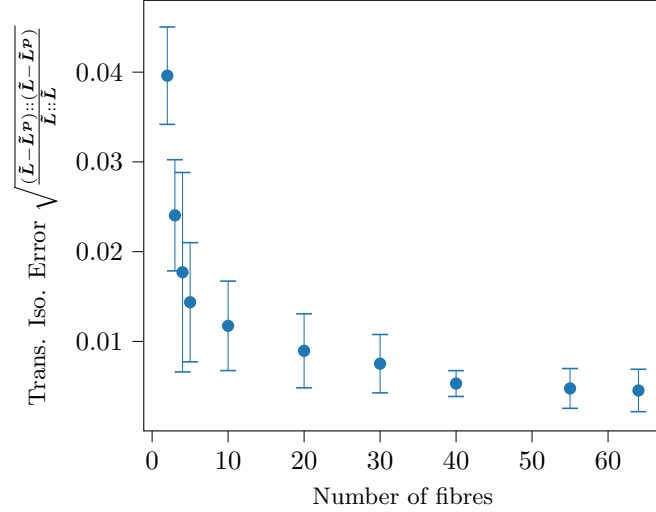


Figure 6: Transverse isotropy error according to the number of fibres - mean and standard deviation based on populations made of 10 RVEs for every size.

3.3. Viscoelastic homogenization results

In this paragraph are shown the linear viscoelastic homogenization results for the reference RVE, the co-fabric RVE and the coated RVE in the case of a steady-state response to a harmonic loading. For this framework, the thermodynamic admissibility of the results was verified: it was found that a sufficient condition to the positivity of the dissipated energy and the mean elastic (i.e. stored) energy for one cycle was the definite positivity of the effective relaxation tensor. This condition directly involves the positivity of both real and imaginary parts of the different complex moduli. Figure 7 shows the complex $\tilde{\alpha}^*$ modulus comparison between the three microstructures. The third graph is the loss factor $\tan \phi$ which is defined as follows:

$$\tan(\phi_{\tilde{\alpha}^*}) = \frac{\tilde{\alpha}'}{\tilde{\alpha}''}. \quad (14)$$

Figure 8 displays the loss factors obtained for the other effective complex moduli ($\tilde{\beta}^*$, $\tilde{\gamma}^*$, $\tilde{\delta}_T^*$ and $\tilde{\delta}_L^*$). We begin by noting that, as expected, the reference RVE, containing no elastomer, exhibits the smallest loss factors of the three RVEs. Moreover, the loss factors obtained for this RVE follow the same trend as the epoxy resin, namely the loss factor decreases with the frequency. At the opposite, the coated RVE shows the highest values for the loss factors of all the moduli and for almost all frequency values. This can be explained by the fact that, in contrary to the co-fabric technology, for the coated technology, the load is transferred from the epoxy matrix to the fibres by the elastomer which undergoes more strain and which therefore dissipates more energy through viscosity. The loss factor associated with the shear moduli $\tilde{\delta}_T^*$ and $\tilde{\delta}_L^*$ is greater than those associated with the other ones, especially at high frequency, because shear is the loading mode for which the elastomer dissipates the most energy, because of its incompressible behaviour. At low frequency, below around 10 Hz, the loss factors associated with the moduli of the coated RVE, except for $\tilde{\delta}_L^*$, increase when the frequency decreases, this evolution is less obvious because it is contrary to that observed for the elastomer taken alone. But this is explained by the strong decrease of the elastomer moduli at low frequencies, in comparison to those of the epoxy matrix, from which results more strain in the elastomer and therefore more energy dissipated. And finally, the loss factor associated to the moduli $\tilde{\alpha}^*$, characterizing the effective behaviour in the fibres direction, is very small because of the very high stiffness contrast between the fibres and the epoxy resin and the elastomer which reduces the strain in these materials and consequently the energy dissipated.

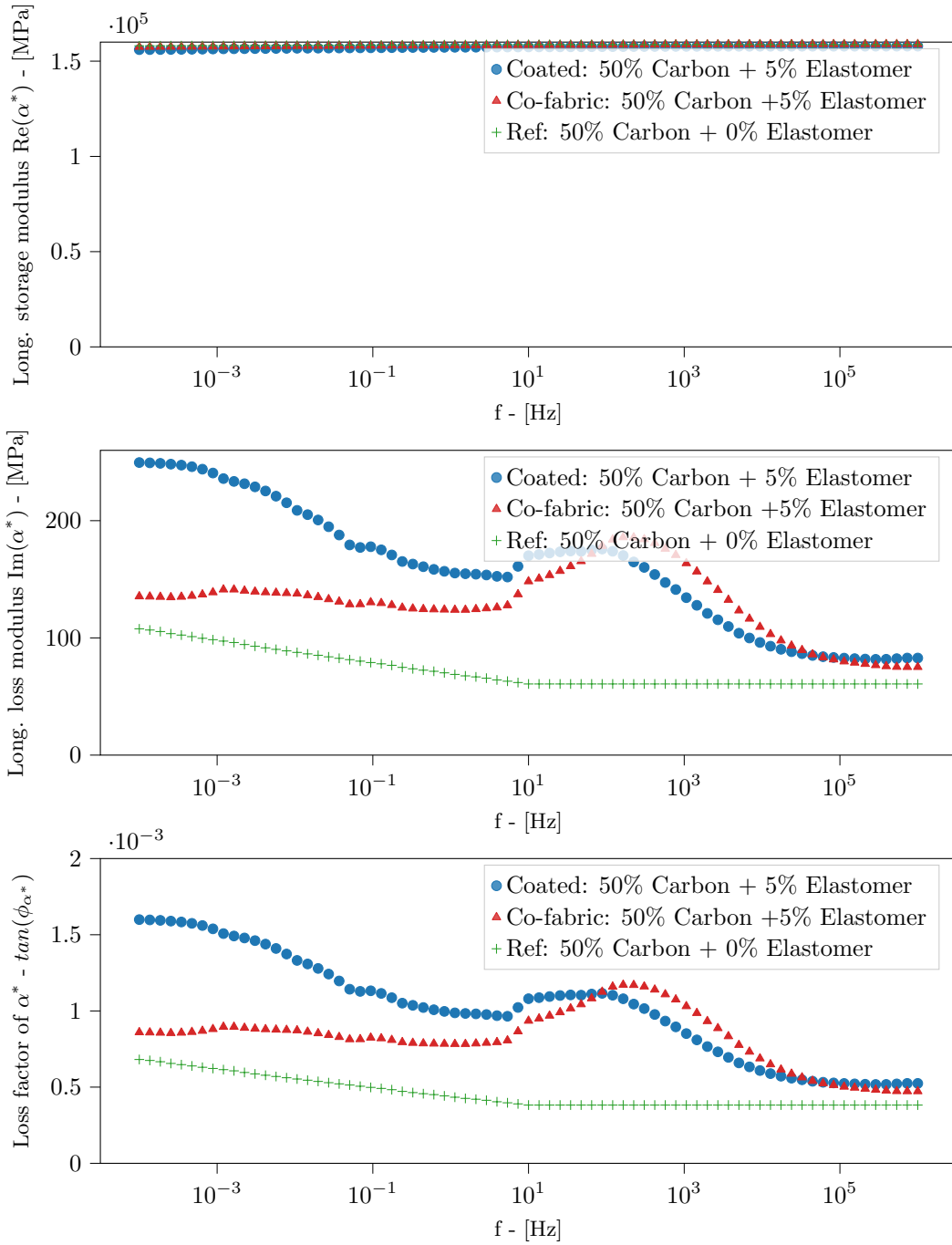


Figure 7: Complex $\tilde{\alpha}^*$ modulus according to frequency of the different UD plies

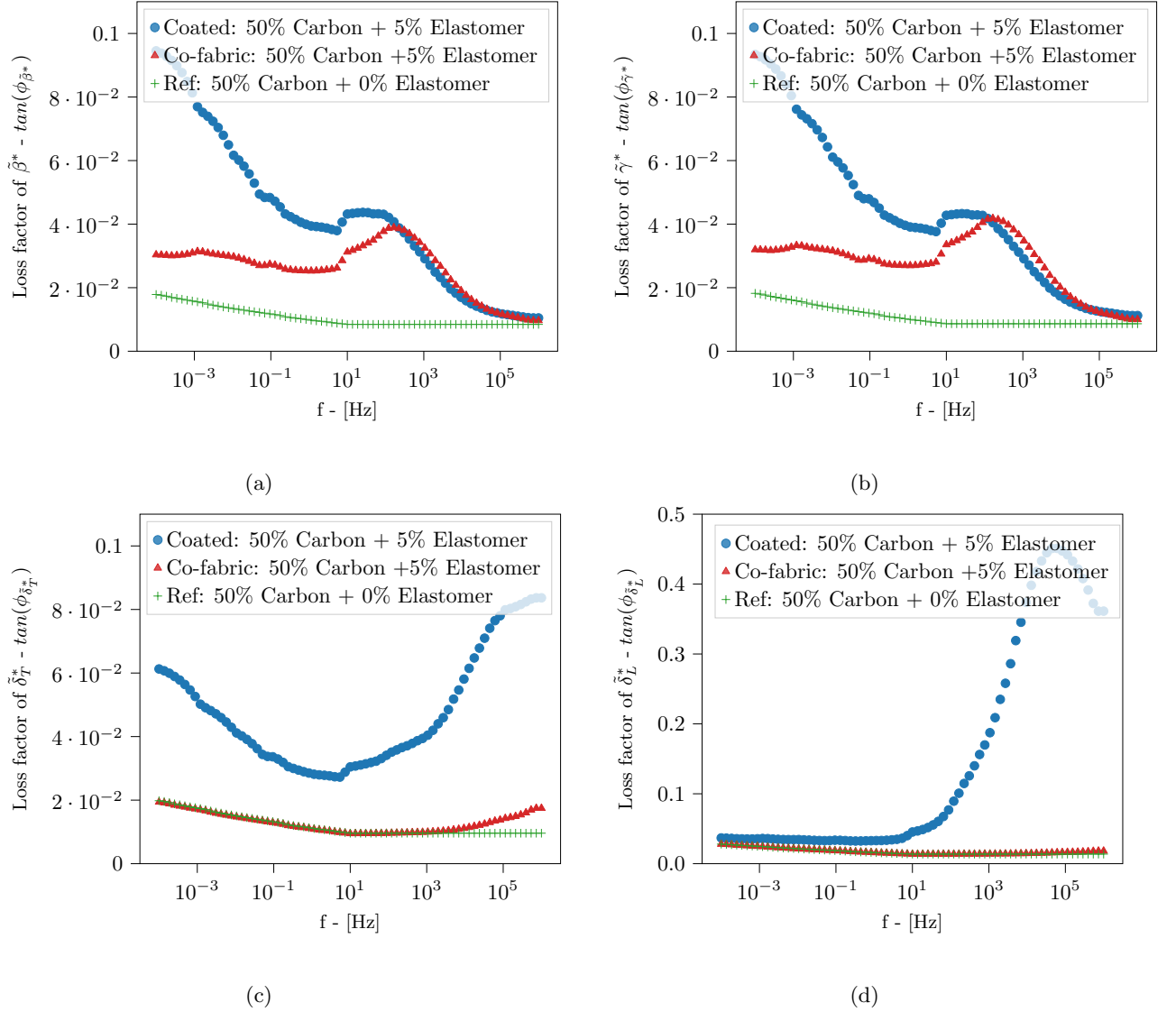


Figure 8: Loss factors for all the other independent coefficients of the effective tensor $\tilde{\mathbf{L}}^*$: β^* , γ^* , δ_T^* and δ_L^*

For every microstructure, the effective complex moduli $\tilde{\alpha}^*$, $\tilde{\beta}^*$, $\tilde{\gamma}^*$, $\tilde{\delta}_T^*$ and $\tilde{\delta}_L^*$ of the viscoelasticity tensor $\tilde{\mathbf{L}}^*$ are extracted in order to be used as inputs for the laminated structures dynamic simulations. To do so, a User Material law was defined. For every frequency step f_i , the real and imaginary parts of the relaxation tensor of each element are computed.

4. Damping properties of laminated structures

4.1. Procedure

Simulations of dynamic cantilever beam bending tests (named Oberst tests in the following) are realised to compare the damping of the first eigenmode of vibration of different laminated structures. As for the homogenization, the simulations are realised using the "Steady-State Dynamics" procedure of FE commercial software Abaqus (as well done in Liebig et al. [31]). To compare the damping capacity of the different hybrid microstructures introduced above, their complex effective behaviours are introduced in different laminated structures:

- One laminate where all the plies are made with the material behaviour resulting from the homogenization of the reference microstructure (without elastomer).
- One laminate where all the plies are made with the material behaviour resulting from the homogenization of the co-fabric microstructure (with 5% elastomer).
- One laminate where all the plies are made with the material behaviour resulting from the homogenization of the coated fibres microstructure (with 5% elastomer).
- One laminate where all the plies are made with the material behaviour resulting from the homogenization of the reference microstructure and an elastomer patch within the plies (the thickness of the elastomer ply is computed such as to introduce the same amount of elastomer in terms of mass as for the previous laminates with elastomer).

In order to quantify the damping of a structure, the damping factor ξ is often computed. The damping factor can be computed using the -3dB graphical method (see Carfagni et al. [7] for more information or more recently Wang et al. [48]) or analytically. A simple analytical method for the determination of damping factor is to consider the response of a 1-D damped harmonic oscillator. In the case of a damped harmonic oscillator submitted to a harmonic loading $F = F_0 \cos(\omega t)$, the response magnitude U can be computed according to radial frequency ω using the formula (15), see Nashif et al. [36] for more theoretical details.

$$U = \frac{F_0/\alpha}{\omega_0^2 \sqrt{(1 - \Omega^2)^2 + (2\xi\Omega)^2}} \quad (15)$$

Where $\Omega = \frac{\omega}{\omega_0}$, ω_0 is the eigen frequency of the undamped harmonic oscillator associated, α is a constant depending on the mass of the system and ξ is the damping factor.

In the case where the different resonant peaks of the displacement magnitude do not overlap, i.e. they are enough far apart in frequency, the equation (15) describes perfectly the resonant peaks of the laminated structures of this study.

Both graphical and analytical methods allow to determine the damping factor successfully. However, the precision of the -3dB graphical method will depend on the frequency sampling of the simulations. The graphical method requires to run simulations with very small sampling periods around resonant peaks, consequently increasing computational times. Therefore, also to reduce computational costs, it is chosen to estimate the damping factor using the analytical model and a curve fitting program. The graphical method is mostly used for damping estimation from experimental data and is actually a simplified case of the analytical method for $\xi \ll 1$. Still, the authors verified that both methods give the same results.

4.2. Experimental validation: Oberst tests

Oberst tests on cantilever beams were performed on UD lay-ups containing an elastomer patch according to the standard **ISO6721-3**. Figure 9 shows the experimental set-up : The excitation shaker is located at the center of the specimen (red circle) while the accelerometers used to measure the specimen response are at both ends of the specimen (green circles). The shaker is an electromagnetic system "964 LS" from LDS (Ling Dynamic System). The specimen size is $300mm \times 20mm$ with a thickness which depends on the stacking sequences, which are shown, together with the patch position, on figure 10 (1.2mm for the simple lay-up called *L0* and 2.6mm for the lay-up *L0 - Elasto - L0*).

The same experiment is performed numerically with the approach illustrated above and the results are compared for the first and second vibration modes. Concerning the boundary conditions defined on the laminates, a harmonic load $F = F_0 \cos(2\pi ft)$, or $F^* = F_0$ in complex notation, was applied on one extremity of the laminate and the other extremity was clamped.

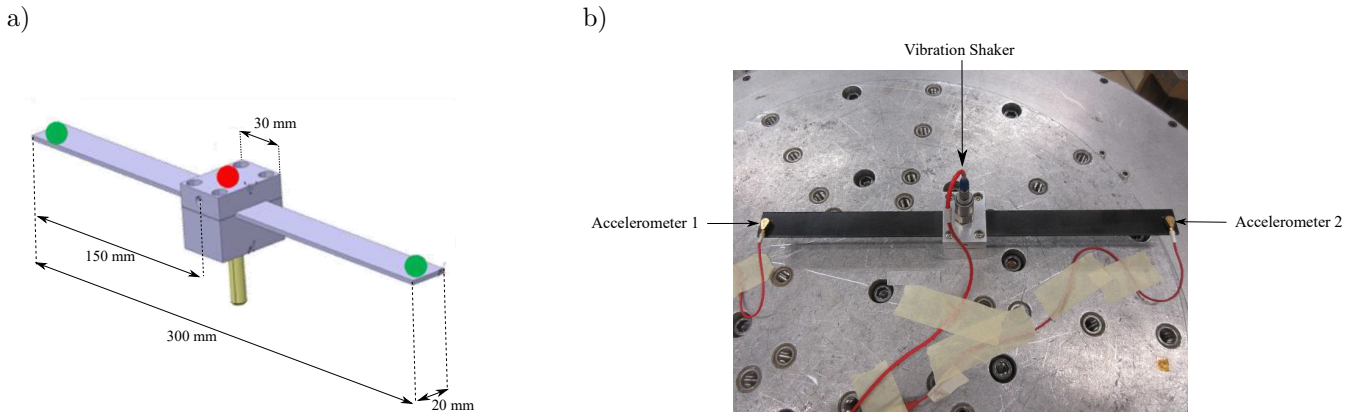


Figure 9: Experimental set-up for the Oberst tests: a) drawing showing the dimensions, b) Picture of the whole set-up with the accelerometers and their cables.

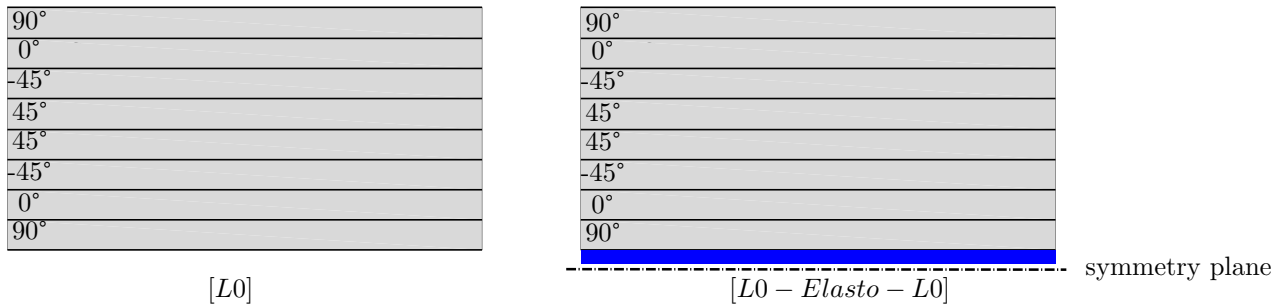


Figure 10: Stacking sequences of the experimental specimens: one 8-ply lay-up without elastomer L0 and one 16-ply lay-up with an elastomer patch in the middle L0-Elasto-L0

Figure 11 shows the resonance peaks of the first vibration modes of the laminates with and without elastomer as illustrated above. The results are presented in the form of graphs where are plotted the normalized response magnitude $|U|/|U|_r$ according to the ratio f/f_r . $|U|_r$ is the maximum displacement value which corresponds to the resonance frequency f_r . This choice is motivated by the fact that the damping factor depends on the inverse of the resonance frequency, therefore using the x-axis f/f_r allows to visually estimate the relative damping of all the laminates by looking at their width at $f/f_r = 1$. Using the y-axis $|U|/|U|_r$ is motivated by the fact that the different laminates don't possess the same rigidity.

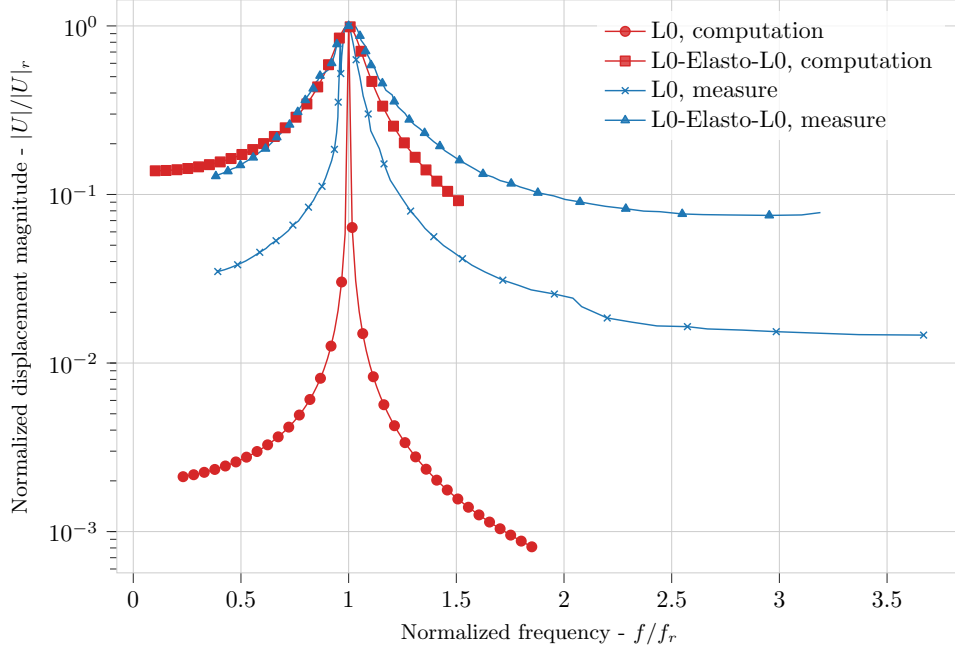


Figure 11: First vibration mode resonance curves for the lay-ups illustrated on figure 10 from experiment and simulation

Lay-up	damping factor ξ	resonance frequency f_r (Hz)
L0 (simulation)	0.0008	43.24
L0 (experiment)	0.029	43.3
L0-Elasto-L0 (simulation)	0.06	97.7
L0-Elasto-L0 (experiment)	0.069	99.6

Table 4: Comparison of damping factors and resonance frequencies measured and computed for the **first vibration mode**

In terms of resonance frequency (see table 4), the simulations give very consistent values compared to the tests results for both laminates. In terms of damping factors, an underestimation of the damping for the laminate L0 is noticeable: it is almost 40 times lower. The most likely hypothesis to explain this difference is the presence of other sources of dissipation in our experimental system, like friction phenomena in the mounting or interactions with the cables linking the accelerometers, see figure9(b), which would distort the damping factor measurement.

As a matter of fact, the value of this damping factor should be near of $\xi = 0.0005$ measured by He et al. [21] for the first eigenmode of a $[0, 90, 45, -45]_{2S}$ CFRP UD laminate, it is clear that the measured one ($\xi = 0.029$) is far too large whereas the simulated one ($\xi = 0.0008$) is of the same magnitude. In contrast, the damping factors estimated for the laminate with elastomer is very close to that measured experimentally. This variability would be lower for the laminate with elastomer since this friction would become negligible compared to the damping of this structure.

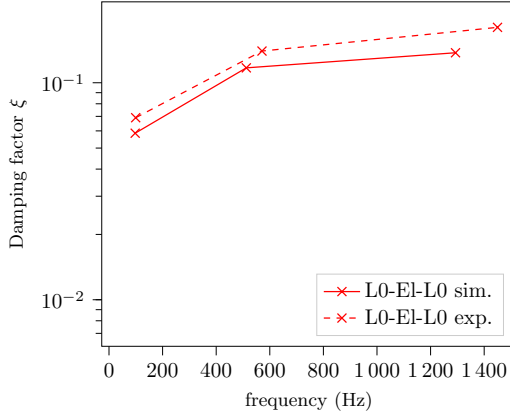


Figure 12: Damping factor vs the three first resonance frequencies. Dashed line for the experiments and continuous lines for the simulations.

Figure 12 shows the damping factor for the three first bending resonance frequencies. We didn't plot in that figure the damping factor measured experimentally for the laminate L0 because, as was said previously, our experimental setup was not able to measure such a low damping values. In terms of resonance frequency, the difference between the numerical estimation and the measured resonance frequency increase with the mode number but remains acceptable regarding the magnitudes. In terms of damping factor of the laminate containing elastomer, the numerical estimate capture very well the increase of the damping factor with the mode number as was already observed by Kishi et al. [26]. Nevertheless, this preliminary results show that the numerical strategy can be considered sufficiently reliable and predictive to compare the response of laminated composite structures subjected to vibrations, especially for laminates containing an elastomer patch.

4.3. Damping technologies comparison

In this paragraph, laminates with the different damping technologies introduced previously are studied and their influence on structural damping factor ξ . Three lay-ups containing the UD carbon plies, the behaviour of which are computed in section 3, are studied for each technologies: $[0]_{8S}$, $[90]_{8S}$ and $[-45, 90, 45, 0]_S$. Concerning the patch technology, two different patch configurations are compared. The first one respects the symmetry of the laminate stacking sequence by introducing the elastomer layer in the middle of the laminate. In the second configuration, the position of the elastomer layer is chosen to be more representative of the target application: it is introduced on top of the laminate and constrained with an additional UD layer as illustrated on figure 13. This additional ply remains oriented at 0° whatever the 8-ply lay-up under is. In any case, the elastomer layer thickness t_e is chosen so that the total volume of elastomer in all the lay-ups remains equal and is equal to 0.056 mm.

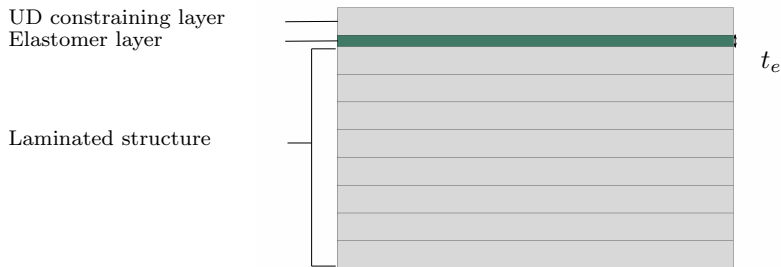


Figure 13: Laminated structure with passive constrained layer damping

Before illustrating some results, it is of first order to remind that adding an additional UD constraining layer in the case of the second patch configuration modifies not only the mass of the structure but also the stiffness, compared to the other technologies (co-fabric and coated) for which only the stiffness varies.

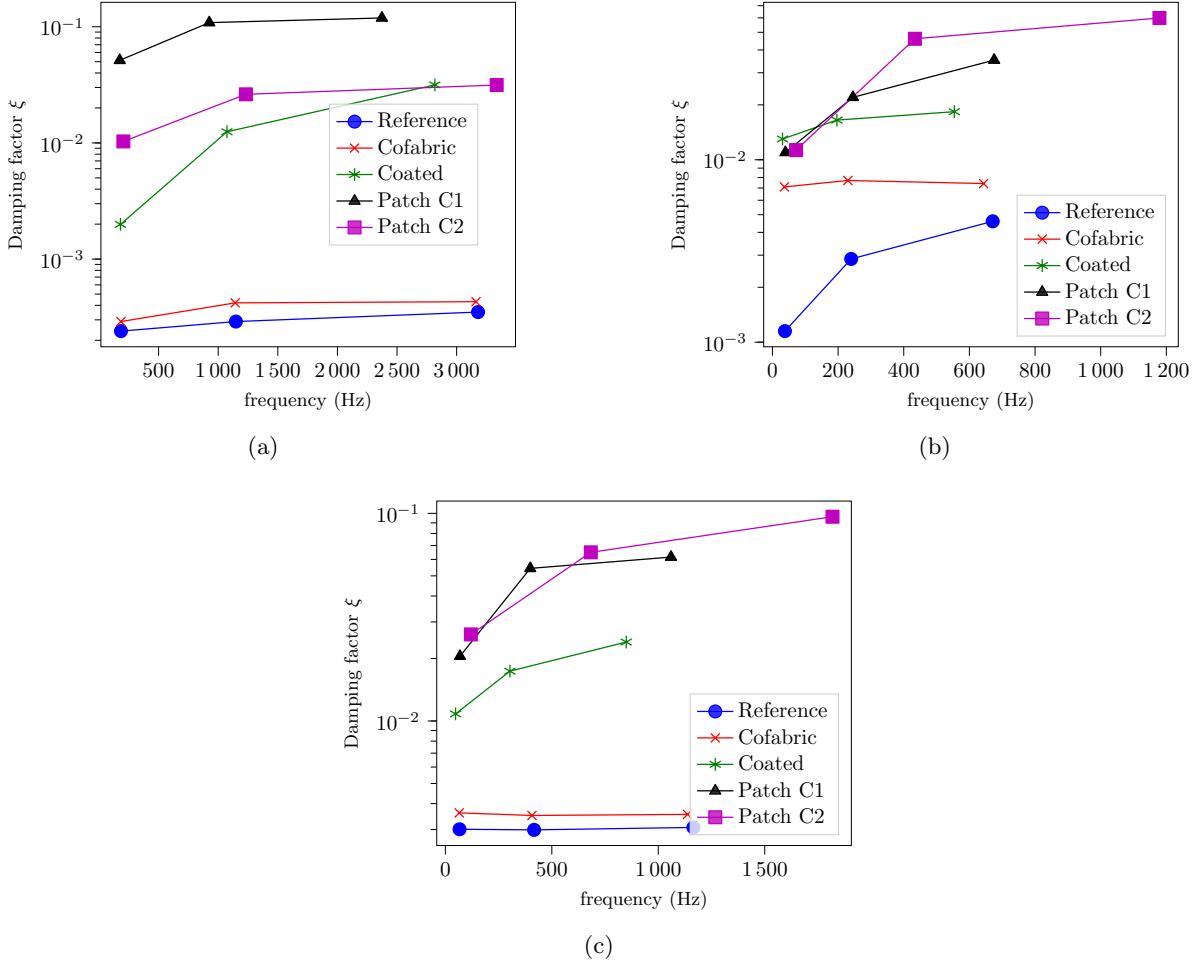


Figure 14: Damping factor vs the three first bending resonance frequencies. (a) $[0]_{8S}$ laminate, (b) $[90]_{8S}$ laminate and (c) the $[-45, 90, 45, 0]_S$ laminate.

On figure 14 are represented the damping factors for the three first bending resonances frequencies of every technology introduced before for the three studied laminates. Not surprisingly the reference laminate, which does not contain elastomer, is the one for which the damping ratio is the lower, for the three first modes and for all the studied lay-up sequences. The value estimated for the first mode of the $[0]_{8S}$ laminate ($\xi=0.00011$) seems to be a little lower than $\xi=0.0006$ obtained by averaging values given in four references for the same lay-up³ but agree perfectly with the one obtained numerically by Kern et al. [25] for similar composite materials. However, the value obtained for the first mode of the $[90]_{8S}$ laminate ($\xi=0.0046$) is very close both to $\xi=0.004$ obtained by averaging the values given for the same lay-up in the reference previously mentioned³ and to that estimated numerically by Kern et al. [25].

The Co-fabric technology brings more damping for the $[90]_{8S}$ laminate than for the other orientations. This has already been noticed by Martone et al. [34], in the context of PU viscoelastic fibres, and can be explain by the high stiffness in the fibres direction which greatly limits the strain in the elastomer fibres

³Yim and Gillespie Jr [50], Kishi et al. [26], Pereira et al. [39] and He et al. [21]

whereas the smaller stiffness in the transverse direction let the elastomer fibres reach more strain amplitude involving more energy dissipation.

For the three studied laminates, the coating technology brings more damping compared to the co-fabric technology with a maximum damping ratio obtained for the $[90]_{8S}$ laminate. This is not surprising since the loss factors of the moduli of the coated RVE are greater than those of the co-fabric RVE, as was discussed in section 3.3. For the $[0]_{8S}$ and the $[90]_{8S}$ laminates, the damping ratios estimated here are greater than those obtained by Kern et al. [25] but in our work the coating is very much thicker. However, as in this last reference, the gain in damping ratio is found greater for the $[0]_{8S}$ than for the $[90]_{8S}$ laminates (more than three times more gain for the $[0]_{8S}$ than for the $[90]_{8S}$).

In contrary to the other technologies, the patch in configuration 1 is more efficient for the stiffest laminates. This has already been experimentally highlighted by Berthelot et al. [3] for UD glass and by Kishi et al. [26] for UD carbon and comes from the increase of the transverse shear applied to the patch with the increase of the stiffness of the plies located on both sides of it. The damping ratios estimated here are difficult to compare with those given in the literature because these values are closely linked to the viscoelastic material constituting the patch, see Kishi et al. [26], as well as to its thickness, see Zheng et al. [51]. Nevertheless, the values $\xi=0.048$ and $\xi=0.008$ obtained for the $[0]_{8S}$ and the $[90]_{8S}$ laminates respectively, seem consistent with those found in the previously cited references.

The results obtained for the patch in configuration 2 are more complex to discuss because the orientation of the constraining ply is different from the other plies. However for the $[0]_{8S}$, the damping estimated for this configuration is lower than that of the configuration 1 because it involve less transverse shear in the viscoelastic patch. But in contrary to the configuration 1, the configuration 2 is more efficient for the $[90]_{8S}$ and especially the $[-45, 90, 45, 0]_S$ laminates. This comes from the stiffness distribution on either side of the patch and show the great interest of the proposed method to estimate the damping of complex structures.

For the three laminates, the simulations estimate an increase of the damping factor with the value of the resonance frequencies except for the Co-fabric technology what was already observed by Kishi et al. [26] for the patch technology and by Kern et al. [25] for the coated technology.

To conclude, for the microscopically tailored laminates (i.e. co-fabric and coated), it appears that the coating technology brings more damping compared to the co-fabric and considering every technology, it appears that the patch technology (configuration 1) brings the highest damping without highly modifying the resonance frequency.

5. Conclusions

Globally, this study enabled to develop a consistent and simple to use numerical tool to estimate the modal damping associated to the first eigenmodes of laminate structures made of CFRP and elastomer. Experimental validation confirmed the robustness for predicting damping factor and resonance frequency for laminates with an elastomer patch. Therefore, from an industrial point of view, it can be used on first stages of structures design in order to define optimum stacking sequences regarding damping and stiffness properties.

Concerning the comparison between the studied damping technologies, it appeared that, for any stacking sequence studied, the laminate which possesses the effective properties of the coated microstructure always shows more damping than the ones with the co-fabric properties. This improvement in damping can also be accompanied with a significant change in stiffness (compared to the reference laminate without elastomer) that depends on the orientation of the laminate plies.

However, regarding all the technologies, it also appeared that the viscoelastic patch is the technology which brings the highest levels of damping but the results will depend on the patch position and the stacking sequence. A criterion on the allowed change of stiffness will define whether the patch can be used or not. Furthermore, consequences on global mechanical strength of the structure have to be investigated and will of course make other design parameters evolve. This study is in reality multiply coupled.

In this study, thermal effects were not taken into account even if thermomechanical couplings can have a strong influence on the elastomer behaviour. It would be interesting to add a thermomechanical behaviour

and to observe how dissipation and therefore damping evolve. Finally, it would also be interesting to consider geometric or materials non-linearities in the model: because of the fact that some aeronautical structures can undergo up to 20% of dynamic deformation (or alternatively can have a high static preload), adding finite strain behaviour seems to be the next interesting simulation effort to make.

References

- [1] Alberola, N., Benzarti, K., Sep. 1997. Méso- et microstructures des composites unidirectionnels: modélisation du comportement viscoélastique. *Comptes Rendus de l'Académie des Sciences - Series IIB - Mechanics-Physics-Chemistry-Astronomy* 325 (5), 249–255.
URL <http://www.sciencedirect.com/science/article/pii/S1251806997883881>
- [2] Bert, C. W., Jul. 1973. Material damping: An introductory review of mathematic measures and experimental technique. *Journal of Sound and Vibration* 29 (2), 129–153.
URL <http://www.sciencedirect.com/science/article/pii/S0022460X73801312>
- [3] Berthelot, J.-M., Assarar, M., Sefrani, Y., El Mahi, A., 2008. Damping analysis of composite materials and structures. *Composite Structures* 85 (3), 189–204.
- [4] Bornert, M., Bretheau, T., Gilormini, P., 2001. Homogénéisation en mécanique des matériaux 1 : matériaux aléatoires élastiques et milieux périodiques.
URL <https://www.lavoisier.fr/livre/materiaux/homogeneisation-en-mecanique-des-materiaux-1-materiaux-aleatoires-elastiques-et-milieux-periodiques>
- [5] Bornert, M., Bretheau, T., Gilormini, P., 2001. Homogénéisation en mécanique des matériaux 2 : comportements non linéaires et problèmes ouverts.
URL <https://www.lavoisier.fr/livre/materiaux/homogeneisation-en-mecanique-des-materiaux-2-comportements-non-lineaires-et-problemes-ouverts>
- [6] Burgarella, B., Maurel-Pantel, A., Lahellec, N., Bouvard, J.-L., Billon, N., 2020. Modeling the effective viscoelastic properties of peek matrix reinforced by arbitrary oriented short glass fibers. *Mechanics of Time-Dependent Materials*, 1–29.
- [7] Carfagni, M., Lenzi, E., Pierini, M., 1998. The loss factor as a measure of mechanical damping. In: *SPIE proceedings series*. pp. 580–584, iSSN: .
- [8] Courtois, A., Jun. 2018. 3D Interlock Composites Multi-Scale Viscoelastic Model Development, Characterization and Modeling. phd, École Polytechnique de Montréal.
URL <https://publications.polymtl.ca/3178/>
- [9] Courtois, A., Hirsekorn, M., Benavente, M., Jaillon, A., Marcin, L., Ruiz, E., Lévesque, M., Jan. 2019. Viscoelastic behavior of an epoxy resin during cure below the glass transition temperature: Characterization and modeling. *Journal of Composite Materials* 53 (2), 155–171, publisher: SAGE Publications Ltd STM.
URL <https://doi.org/10.1177/0021998318781226>
- [10] Dealy, J., Plazek, D., Jan. 2009. Time-temperature superposition-a users guide. *Rheol. Bull.* 78, 16–31.
- [11] Diani, J., Gilormini, P., Oct. 2017. On necessary precautions when measuring solid polymer linear viscoelasticity with dynamic analysis in torsion. *Polymer Testing* 63, 275–280.
URL <http://www.sciencedirect.com/science/article/pii/S0142941817309492>
- [12] El Hachemi, M., Koutsawa, Y., Nasser, H., Giunta, G., Daouadji, A., Daya, E., Belouettar, S., 2016. An intuitive computational multi-scale methodology and tool for the dynamic modelling of viscoelastic composites and structures. *Composite Structures* 144, 131–137.
- [13] El Mourid, A., Ganesan, R., Lévesque, M., Mar. 2013. Comparison between analytical and numerical predictions for the linearly viscoelastic behavior of textile composites. *Mechanics of Materials* 58, 69–83.
URL <http://www.sciencedirect.com/science/article/pii/S0167663612001974>
- [14] Ferry, J. D., Sep. 1980. *Viscoelastic Properties of Polymers*. John Wiley & Sons, google-Books-ID: 9dqQY3Ujsx4C.
- [15] Finegan, I. C., Gibson, R. F., Apr. 1998. Improvement of Damping at the Micromechanical Level in Polymer Composite Materials Under Transverse Normal Loading by the Use of Special Fiber Coatings. *Journal of Vibration and Acoustics* 120 (2), 623–627.
URL <https://doi.org/10.1115/1.2893872>
- [16] Gallican, V., Brenner, R., 2019. Homogenization estimates for the effective response of fractional viscoelastic particulate composites. *Continuum Mechanics and Thermodynamics* 31, 823–840.
URL <https://hal.archives-ouvertes.fr/hal-02023868>
- [17] Gao, F., Song, H., Qiu, X., He, F., Shi, C., Zhao, N., He, C., 2019. The preparation and properties of novel structural damping composites reinforced by nitrile rubber coated 3-D braided carbon fibers. *Polymer Composites* 40 (S1), E599–E608, eprint: <https://onlinelibrary.wiley.com/doi/pdf/10.1002/pc.24905>.
URL <https://onlinelibrary.wiley.com/doi/abs/10.1002/pc.24905>
- [18] Gurtin, M. E., Sternberg, E., Jan. 1962. On the linear theory of viscoelasticity. *Archive for Rational Mechanics and Analysis* 11 (1), 291–356.
URL <https://doi.org/10.1007/BF00253942>
- [19] Gusev, A. A., Sep. 1997. Representative volume element size for elastic composites: A numerical study. *Journal of the Mechanics and Physics of Solids* 45 (9), 1449–1459.
URL <http://www.sciencedirect.com/science/article/pii/S0022509697000161>
- [20] Hashin, Z., 1970. Complex moduli of viscoelastic composites—i. general theory and application to particulate composites. *International Journal of Solids and Structures* 6 (5), 539–552.
- [21] He, Y., Xiao, Y., Liu, Y., Zhang, Z., 2018. An efficient finite element method for computing modal damping of laminated composites: theory and experiment. *Composite Structures* 184, 728–741.
- [22] Hwang, S. J., Gibson, R. F., Jan. 1993. Prediction of fiber-matrix interphase effects on damping of composites using a micromechanical strain energy/finite element approach. *Composites Engineering* 3 (10), 975–984.
URL <http://www.sciencedirect.com/science/article/pii/0961952693900055>
- [23] Jones, D. I. G., Feb. 1996. Reflexion on damping technology at the end of the twentieth century. *Journal of Sound and*

- Vibration 190 (3), 449–462.
URL <http://www.sciencedirect.com/science/article/pii/S0022460X96900735>
- [24] Kanit, T., Forest, S., Galliet, I., Mounoury, V., Jeulin, D., Jun. 2003. Determination of the size of the representative volume element for random composites: statistical and numerical approach. *International Journal of Solids and Structures* 40 (13), 3647–3679.
URL <http://www.sciencedirect.com/science/article/pii/S0020768303001434>
- [25] Kern, L. S., Hine, P. J., Gusev, A. A., 2019. Optimizing the damping properties of unidirectional composites by incorporating carbon fibers with a thin viscoelastic coating. *Composite Structures* 208, 879–890.
- [26] Kishi, H., Kuwata, M., Matsuda, S., Asami, T., Murakami, A., Dec. 2004. Damping properties of thermoplastic-elastomer interleaved carbon fiber-reinforced epoxy composites. *Composites Science and Technology* 64 (16), 2517–2523.
URL <http://www.sciencedirect.com/science/article/pii/S0266353804001393>
- [27] Knauss, W. G., Emri, I., Lu, H., 2008. *Mechanics of Polymers: Viscoelasticity*. In: Sharpe, W. N. (Ed.), *Springer Handbook of Experimental Solid Mechanics*. Springer Handbooks. Springer US, Boston, MA, pp. 49–96.
- [28] Kulhavy, P., Petru, M., Syrovatková, M., Sep. 2017. Possibilities of the Additional Damping of Unidirectional Fiber Composites by Implementation of Viscoelastic Neoprene and Rubber Layers. ISSN: 1070-9622 Pages: e4163485 Publisher: Hindawi Volume: 2017.
URL <https://www.hindawi.com/journals/sv/2017/4163485/>
- [29] Lakes, R. S., Mar. 2004. Viscoelastic measurement techniques. *Review of Scientific Instruments* 75 (4), 797–810, publisher: American Institute of Physics.
URL <https://aip.scitation.org/doi/10.1063/1.1651639>
- [30] Lejeunes, S., Bourgeois, S., 2011. Homtools: an abaqus toolbox for the computation of effective properties of heterogeneous media. In: *proceedings of the 10th National Conference on Computation methods for Structures*. Giens, France.
URL <http://homtools.lma.cnrs-mrs.fr/>
- [31] Liebig, W. V., Jackstadt, A., Sessner, V., Weidenmann, K. A., Kärger, L., 2019. Frequency domain modelling of transversely isotropic viscoelastic fibre-reinforced plastics. *Composites Science and Technology* 180, 101–110.
- [32] Marshall, J. G., Imregun, M., Apr. 1996. a review of aeroelasticity methods with emphasis on turbomachinery applications. *Journal of Fluids and Structures* 10 (3), 237–267.
URL <https://www.sciencedirect.com/science/article/pii/S0889974696900158>
- [33] Martinez-Agirre, M., Illescas, S., Elejabarrieta, M. J., 2014. Characterisation and modelling of prestrained viscoelastic films. *International Journal of Adhesion and Adhesives* 50, 183 – 190.
URL <http://www.sciencedirect.com/science/article/pii/S014374961400030X>
- [34] Martone, A., Giordano, M., Antonucci, V., Zarrelli, M., Nov. 2011. Enhancing damping features of advanced polymer composites by micromechanical hybridization. *Composites Part A: Applied Science and Manufacturing* 42 (11), 1663–1672.
- [35] Milton, G., 03 2003. Theory of Composites. *Applied Mechanics Reviews* 56 (2), B27–B28.
URL <https://doi.org/10.1115/1.1553445>
- [36] Nashif, A. D., Jones, D. I. G., Henderson, J. P., Mar. 1985. *Vibration Damping*. John Wiley & Sons, google-Books-ID: oE11HAXHg4AC.
- [37] Noûs, C., Boisse, J., André, S., May 2021. An FFT solver used for virtual Dynamic Mechanical Analysis experiments: Application to a glassy/amorphous system and to a particulate composite. *Journal of Theoretical, Computational and Applied Mechanics* Publisher: Episciences.org.
URL <https://jtcam.episciences.org/7456/pdf>
- [38] O’Brien, D. J., Mather, P. T., White, S. R., May 2001. Viscoelastic Properties of an Epoxy Resin during Cure. *Journal of Composite Materials* 35 (10), 883–904, publisher: SAGE Publications Ltd STM.
URL <https://doi.org/10.1177/a037323>
- [39] Pereira, D., Guimarães, T., Resende, H., Rade, D., 2020. Numerical and experimental analyses of modal frequency and damping in tow-steered cfrp laminates. *Composite Structures* 244, 112190.
- [40] Pritz, T., Jul. 2000. Measurement methods of complex Poisson’s ratio of viscoelastic materials. *Applied Acoustics* 60 (3), 279–292.
URL <http://www.sciencedirect.com/science/article/pii/S0003682X99000493>
- [41] Rougier, Y., Stolz, C., Zaoui, A., 1993. Représentation spectrale en viscoélasticité linéaire des matériaux hétérogènes.
- [42] Roylance, D., 2001. *ENGINEERING VISCOELASTICITY*, 38.
- [43] Schapery, R., 1967. Stress analysis of viscoelastic composite materials. *Journal of Composite Materials* 1 (3), 228–267.
- [44] Swolfs, Y., Verpoest, I., Gorbatikh, L., 2019. Recent advances in fibre-hybrid composites: materials selection, opportunities and applications. *International Materials Reviews* 64 (4), 181–215.
- [45] Torquato, Haslach, Jul. 2002. Random Heterogeneous Materials: Microstructure and Macroscopic Properties. *Applied Mechanics Reviews* 55 (4), B62–B63, publisher: American Society of Mechanical Engineers Digital Collection.
URL <https://asmedigitalcollection.asme.org/appliedmechanicsreviews/article/55/4/B62/458303/Random-Heterogeneous-Materials>
- [46] Tschöegl, N., Knauss, W. G., Emri, I., Mar. 2002. Poisson’s Ratio in Linear Viscoelasticity – A Critical Review. *Mechanics of Time-Dependent Materials* 6 (1), 3–51.
URL <https://doi.org/10.1023/A:1014411503170>
- [47] Vahdati, M., Lee, K.-B., Sureshkumar, P., 2020. A Review of Computational Aeroelasticity Of Civil Fan Blades. *International Journal of Gas Turbine, Propulsion and Power Systems* 11 (4), 22–35.
- [48] Wang, A., Wang, X., Xian, G., Dec. 2021. The influence of stacking sequence on the low-velocity impact response and damping behavior of carbon and flax fabric reinforced hybrid composites. *Polymer Testing* 104, 107384.
URL <https://www.sciencedirect.com/science/article/pii/S0142941821003299>

- [49] Williams, M. L., Landel, R. F., Ferry, J. D., Jul. 1955. The Temperature Dependence of Relaxation Mechanisms in Amorphous Polymers and Other Glass-forming Liquids. *Journal of the American Chemical Society* 77 (14), 3701–3707.
URL <https://doi.org/10.1021/ja01619a008>
- [50] Yim, J. H., Gillespie Jr, J. W., Nov. 2000. Damping characteristics of 0° and 90° AS4/3501-6 unidirectional laminates including the transverse shear effect. *Composite Structures* 50 (3), 217–225.
URL <http://www.sciencedirect.com/science/article/pii/S0263822300000878>
- [51] Zheng, C., Duan, F., Liang, S., 2021. Manufacturing and mechanical performance of novel epoxy resin matrix carbon fiber reinforced damping composites. *Composite Structures* 256, 113099.